Li Intercalation into Graphite: Direct Optical Imaging and Cahn–Hilliard Reaction Dynamics

Li Intercalation into Graphite: Direct Optical Imaging and Cahn-Hilliard Reaction Dynamics

Yinsheng Guo[1], Raymond B. Smith[2], Zhonghua Yu[1], Dmitri K. Efetov[3], Junpu Wang[3], Philip Kim[3], Martin Z. Bazant[2, 4], Louis E. Brus[1]

[1]Department of Chemistry and [3]Department of Physics, Columbia University, New York, 10027, United States

[2]Department of Chemical Engineering and [4]Department of Mathematics, Massachusetts Institute of Technology, Cambridge, Massachusetts, 02139, United States

ABSTRACT

Lithium intercalation into graphite is a critical process in energy storage technology. Studies of Li intercalation kinetics have proved challenging due to structural and phase complexity, and sample heterogeneity. Here we report direct time- and space-resolved, all-optical measurement of Li intercalation. We use a single crystal graphite electrode with lithographically defined disc geometry. All-optical, Raman and reflectance measurements distinguish the intrinsic intercalation process from side reactions, and provide new insight into the microscopic intercalation process. The recently proposed Cahn-Hilliard reaction

(CHR) theory quantitatively captures the observed phase front spatial patterns and dynamics, using a two-layer free-energy model with novel, generalized Butler-Volmer kinetics. This approach unites Cahn-Hilliard and electrochemical kinetics, using a thermodynamically consistent description of the Li injection reaction at the crystal edge that involves a cooperative opening of graphene planes. The excellent agreement between experiment and theory presented here, with single-crystal resolution, provides strong support for the CHR theory of solid-state reactions.

Table of Contents Graphic and Synopsis

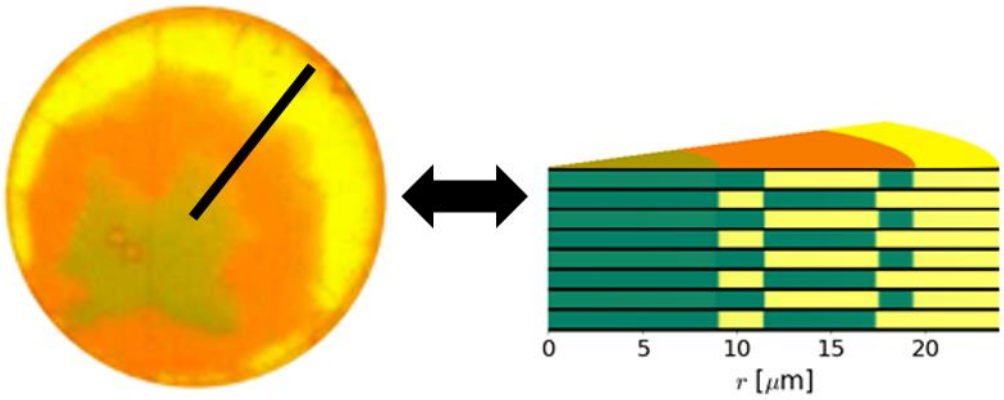

KEYWORDS

Intercalation kinetics, optical reflectance, Raman spectroscopy, Cahn-Hilliard Reaction Dynamics, graphite, lithium, solid-solid phase transition

TEXT

Graphite intercalation compounds (GICs) are stoichiometric, thermodynamically stable materials in which graphite in-plane electrical conductivity is significantly increased by electron or hole doping from species between layers .[1] Lithium intercalated graphite shows a rich phase diagram and is widely used as the anode in batteries and other electrochemical energy storage systems. Understanding Li intercalation is a critical technological problem that has been studied principally using electrochemical methods: [2–8] potentiostatic intermittent titration (PITT), galvanostatic intermittent titration (GITT), electrochemical impedance spectroscopy (EIS), and slow scan rate cyclic voltammetry(CV). Additional information on elementary atomic hopping steps of Li transport has also been obtained from nuclear magnetic resonance.[9]

While these methods yield valuable insight, electrical measurements alone cannot uniquely specify the kinetics.[3,7] Electrical measurements couple the sequential formation of different GIC phases with Li^+ transport in the electrolyte, interfacial (electrolyte/graphite) Li^+ injection, and side redox reactions. Moreover, common graphite anodes are inhomogeneous, consisting of heterogeneous graphite particles connected by polymer binders. In such samples, phase nucleation and growth, as a function of increasing Li concentration, is wildly heterogeneous,[10] as also observed in phase-separating Li-ion battery porous cathodes.[11–13] As a result of these and other complications[27], reported values of the Li diffusion coefficient inside graphite vary by about 10 orders of magnitude, from 10^{-6} to 10^{-16} cm^2/s.[4,14]

We report direct all-optical reflectance imaging of Li intercalation kinetics into a lithographically defined, single crystal of bulk graphite. Classical diffusion models fail to capture the propagating phase fronts and concentration profiles, but we show, for the first time, that the recently developed Cahn-Hillard reaction (CHR) theory of non-equilibrium phase separating systems[24,26] can quantitatively describe our observations, using a periodic two-layer free energy

model[27] with novel generalized Butler-Volmer kinetics. Strong Li interactions create alternating, distinct Li concentrations between adjacent graphene layers that form three stable phases: both layers full, both empty, and alternating full and empty layers in checkerboard patterns. The model allows us to infer a cooperative intercalation reaction mechanism, which depends critically on Li concentration in graphite near the interface.

Optical images of Li intercalation ,[15,16] some into single crystal graphite[9,14] have been previously reported. However, these studies were electrochemical in nature, in that their quantitative conclusions were based on electrochemical current-voltage measurements. They were also interpreted within a diffusion framework.

Observation and Simulation

Intercalation is initiated by a voltage step, which charges the graphite negatively. Li ions are injected at the crystal edge from the electrolyte. At low Li concentration, there is a dilute solid solution of Li in graphite with isolated Li species distributed across all graphene layers. As the concentration increases, regions of fixed local structure and stoichiometry (phases or stages) form. The stage number *n* in Figure 1 is the number of graphene layers without intercalated Li between two complete, crystalline intercalated Li monolayers. The GIC undergoes first order phase transitions through a sequence of dilute stage 1', stage 4, stage 3, stage 2 and finally stage 1[17,18]. Stage 1 (stoichiometric LiC_6) has an intercalated Li crystalline monolayer between every graphene sheet. Electrical and optical properties are strongly dependent on in-plane ordering and stage number.

Figure 2 shows the sequential optical reflection images observed during intercalation into a 50μm diameter single crystal graphite disc (device schematic in supporting information). GIC

stages exhibit distinct colors, resulting from the increasing density of delocalized Drude in-plane graphene metallic electrons donated by intercalated Li. With increasing Li concentration, the Drude plasma edge shifts into the visible from the infrared.[19–22] Stage 3 is green, stage 2 is red, and stage 1 is golden; these assignments are confirmed by in-situ Raman spectroscopy (supporting information) and agree well with previous reports[23]. The entire intercalation sequence is reversible if voltage is reduced to zero.

We can distinguish different kinetic regimes in these images. When Li diffusion from the edge to the center is fast with respect to Li interface injection at the edge, and when the internal concentrations are not within the miscibility gap, the Li concentration is uniform across the entire disk. This occurs in dilute stage 1'as concentration increases; the graphite gradually and uniformly darkens. Darkening reflects the reduction of free carrier lifetime in the presence of random distributed Li. Next, nucleation of green phase 3 occurs homogeneously across the disc.

However, the red colored stage 2 phase subsequently nucleates at the boundary of the disk (Fig. 2c). This indicates that Li transport through stoichiometric stage 2, to the stage 3/stage 2 boundary moving towards the center, is slower than the initial diffusion in dilute stage 1'. Furthermore, nucleation of golden stage 1 occurs almost immediately at the edge after stage 2 forms. The system is out of equilibrium, building up high Li concentration at the edge, as evidenced by the fact that three different phases (3, 2, and 1) are observed simultaneously. Only two phases (2 and 1 for $x>0.5$ in Li_xC_6) exist simultaneously in the equilibrium phase diagram.[18] As the phase boundaries propagate towards the disk center, green phase 3 disappears first, followed by stage 2, leaving only stage 1.

After stage 3 forms, the total Li content in the graphite disk can be obtained directly from the images. The Li content in each phase is the geometrical area multiplied by the Li density from

stoichiometry. The sum from all phases is the total Li content in Figure 3A. The dotted line represents the growth of dilute stage 1'and stage 3. The first data point corresponds to the first image showing the boundary between stage 3 and stage 2. The injection rate of Li at the circumference, (i.e., the slope of the total Li content curve) slows down as Li becomes more concentrated. This kinetic measurement from optical reflectivity is free from other complicating simultaneous electrochemical processes that consume Li. Indeed we observed "blue film" formation around the electrodes resulting from chemical reduction of the polymer electrolyte, as reported by previous workers.[10]

While the initial formation of dilute stage 1' involves diffusion of Li from the edge, the formation of the more concentrated phases is a complex problem of solid state chemical kinetics. Existing intercalation models assume that diffusion within each phase is rate-limiting[6,24,25 26], as originally discussed by Wagner[27] and used to interpret electrochemical measurements, but this is only valid for solid solutions. Naïve application of the diffusion equation cannot capture the spontaneous formation of phase boundaries upon phase separation, nor capture the alternating stage 2 structure. More generally, transport is driven by free energy gradients. Our system is out of equilibrium and exhibits stoichiometric phase formation from strong interaction among Li atoms, both in-plane and across graphene layers. To capture these aspects, we adapt the Cahn-Hillard reaction (CHR) theory of Bazant and coworker**s**[11,28,29] for graphite with a periodic two-layer regular solution model[27] and a new formulation of cooperative intercalation kinetics. Details of the theory will be published elsewhere, but the key ideas are summarized here with equations in the Supplemental Information.

Our free energy model for Li/graphite GICs postulates separate Li concentrations in adjacent Li layers, allowing us to capture Stages 1', 2, and 1. Attractive interactions between intralayer Li are caused by deformations of the surrounding graphene planes; we represent intralayer Li as a regular

solution with an attractive interaction parameter. Each layer has a term penalizing internal concentration gradients, representing interfacial energy between high- and low-lithium phases. We energetically penalize nearby high concentrations in both layers with a parameter representing direct repulsive elastic interaction. Finally we penalize intermediate filling in nearby layers with a dipole-dipole repulsion parameter, which is chosen to be large enough to avoid homogeneous filling behavior. These free energy parameters are taken from previous work on the equlibrium phase diagram[12]. We use an individual Li ion diffusivity, in dilute stage 1', slightly adjusted from *ab initio* calculations of Li diffusion in graphite[3].

In addition to Li transport within the graphite, we find that Li injection kinetics also affected the overall dynamics. We relate the Li injection flux to the electrochemical free energy change with a generalized Butler-Volmer equation that depends upon the electrochemical potentials of the oxidized and reduced states as well as the activity coefficient of the transition state. We specify the activity coefficient of the transition site by postulating its lattice configuration in Figure 4. Li injection is favored when there is an available (empty) site near an occupied site at the surface in the same layer. A nearby intersititial Li (occupied site) helps injection into the empty site by separating the graphene layers. Completely filled/empty layers cost more energy for injection and inhibit reaction compared with half-filled layers. This postulated cooperativity determines how injection depends upon Li concentration. The overall magnitude of the injection rate is left as the only adjustible factor to fit the data.

Computer simulation (Figure 5 and a movie in supplemental) shows each intralayer region spontaneously separating into Li-rich and Li-poor phases, forming a "checkerboard" pattern, much like the schematic originally proposed by Daumas and Hérold[30] and supported by some modeling [31–33] and experimental[34–36] studies. The simulation closely matches the observed kinetics.

Discussion and the Diffusion Approximation

We have described a free energy model which, when coupled with extended Cahn-Hillard reaction dynamics and a simple, physically motivated Li injection model, captures both the non-equilibrium motion of lithiated graphite phase boundaries and the checkerboard distribution of Li in the Stage II region. Although we do not explicitly model local deformations to account for elastic strain effects, the energetic attraction and repulsion terms partially account for local stress effects of stage formation.[37] In addition, graphite has transverse isotropy within the modeled planes,[38] so the effect of in-plane strains would primarily simply enhance the transport rate and broaden the observed interfaces.[39] Because the system is not clamped from above, we also postulate that c-axis strains could relieve stress, which could explain why we did not find it necessary to explicitly describe elastic effects to capture the phase propagation dynamics.

The injection model (adapted from previous work[28]) describes the proposed cooperative mechanism in Figure 4, in which intercalation requires both occupied and unoccupied sites near the crystal surface to proceed. This reaction model gave the best comparison to data among several reasonable possibilities (see supporting information). Thus the injection reaction directly impacts the overall dynamics. Although internal transport clearly limits the process at late times as the lithium transports the 25 μm to the center of the disc, the specifics of the injection resistance are important to capture the experimental results. These free energy and injection models provide a framework that can also be used in other non-equilibrium situations such as practical battery discharge at constant current, or even full porous electrode simulations[11,13].

Other, more involved thermodynamic treatments[40] can predict higher stage number structures. Our simplified model allows for both complete simulation of highly non-equilibrium dynamics as

described above, and limiting analysis of near-equilibrium cases. For example, near equilibrium when concentration gradients are small, our model predicts ranges for the chemical diffusivity within each of the two modeled layers, $D_{chem,1}$ and $D_{chem,2}$ (see supplemental). At room temperature, we find equilibrium Stage 1 and 1' phases have $D^{eq}_{chem,1} = D^{eq}_{chem,2} \approx 1 * 10^{-8}$ cm^2/s. Thus, in near-equilibrium Stage 1 and 1' phases, the total flux, *F*, can be simply related to the gradient in the average concentration, *c*,

$$F = -\mathrm{D}^{\mathrm{eq}}_{\mathrm{chem},1}\nabla\overline{c}. \qquad (15)$$

However, in the Stage 2 region, analysis is not as straightforward because the predicted $D^{eq}_{chem,1} \neq D^{eq}_{chem,2}$. In addition, in a system in which Stage 1', 2, and 1 are all present, the values of $D^{eq}_{chem,1}$ and $D^{eq}_{chem,2}$ must vary over the Stage 2 region as the concentration in that region varies from that in equilibrium with Stage 1' to that in equilibrium with Stage 1. Nevertheless, the two stage 2 layers' equilibrium chemical diffusivities range from $9 * 10^{-9}$ to $1.2 * 10^{-8}$ cm^2/s, which provides a similar scale for the transport in Stage 2. Although these numbers can provide a useful intuition about near-equilibrium transport, it is worth noting that such approximations likely fail in typical battery operations which are often far from equilibrium. Adequate descriptions of such situations require the full extended Cahn-Hillard reaction dynamics.

In summary, with all-optical measurments we unambiguously determine the kinetics of Li injection into a large graphite single crystal, free of interference from electrochemical side reactions. Lithgraphyically defined single crystal experiment allows mechanistic examination by physically founded theory. We show that the recently developed CHR theory can quantitatively describe the *non-equilibrium* kinetics of propagating phase fronts in a single crystal. A cooperative electrochemical model for Li injection at the crystal edge reproduces the overall kinetics. We use an internal Li/graphite free energy that previously was shown to reproduce the *equilibrium*

Li/graphite phase diagram(ref 26). Our studies provide strong evidence to support the CHR approach to both solid-state structure and dynamics.

Methods

Sample preparation and device fabrication

Bulk Kish graphite samples were mechanically exfoliated onto a Si substrate with 285nm thermal oxide, and selected by visual inspection through an optical microscope.[41] A ~100 nm thick chromium mask was defined by standard electron-beam (e-beam) lithography and deposited by e-beam evaporation. Reactive ion etching with O_2 plasma was carried out to shape the underlying graphite sample, followed by the removal of chromium mask with chrome etchant. This process created disk shaped graphite crystals of 50μm diameter. Their thickness was larger than 100nm, the optical skin depth in graphite,[19] as confirmed by the absence of Si modes in measured Raman spectra. Ti contacts was defined by a second round of e-beam lithography and deposited by e-beam evaporation. Ti was chosen as the metal contact to utilize its dense native oxide layer for passivation.[42] After lift-off in acetone bath, the device was wire bonded to a chip carrier. At the side of the device, a blank Si substrate with e-beam evaporated Ti was also wire bonded to the chip carrier. This served as a contact pad for attaching the Li counter/reference electrode.

Anhydrous $LiClO_4$, Polyethylene oxides PEO, and anhydrous acetonitrile were purchased from Sigma Aldrich. $LiClO_4$ and PEO were mixed to achieve a molar ratio of about 36:1 [CH2-CH2-O]/Li^+ and dissolved in 10mL acetonitrile.[43] A typical amount of 5 μl was applied to the device area under a stereo microscope. After the acetonitrile evaporated, a flat and transparent polymer electrolyte film formed, with a thickness on the order of 1um. A fresh-cut, mm-sized Li strip was brought into contact with the polymer electrolyte. Bulk Li metal was used as counter and reference

electrode. The spatial separation between the bulk Li electrode and the lithographically defined graphite sample was on the order of 1mm. The Li strip was attached to the Ti covered blank Si substrate on the side. The assembled device was transferred into an optical cryostat and sealed. The entire process of electrolyte preparation and device assembly was performed in a glove box. H_2O and O_2 concentrations in the glove box were maintained below 1ppm. The electrolyte and Li electrode were not in contact with ambient atmosphere at any time.

Instrumentation and characterization

After assembly the optical cryostat was taken out of the glove box and connected to a turbo pump. The pressure inside the sample chamber was at the level of 10^{-5} torr. The cryostat was also electrically connected to a temperature controller. The temperature was maintained at 338 K. The optical cryostat was mounted on a home built micro Raman setup using the 514nm line of an Argon ion laser. For optical microscopy a quartz tungsten halogen lamp was used for illumination. An imaging camera was controlled by LabVIEW and recorded the micrograph at fixed time intervals. A PARSTAT 2263 potentiostat and Yokogawa GS 200 voltage and current source were used as DC voltage sources.

Data Analysis

Each micrograph image was registered by a translation operation to account for spatial drifting during the experiment. The processed images were segmented with a color based K-means clustering algorithm[44]. Segmentation in Lab color space and RGB color space were performed. RGB color space was used since it gave a cleaner segmentation under our experimental conditions. The total number of pixels contained in each segment was recorded as a direct measurement of the area of a given stage n.

Numerical Simulations

Constant voltage simulations were carried out in time and one spatial (radial) dimension, assuming cylindrical geometry with radial symmetry. Finite volume discretization was used in space with minor modifications for geometry following the reference[29]. Time integration was carried out using DAE Tools[45], which wraps the SUNDIALS integration suite[46] with the ADOL-C automatic differentiation library[47]. With 350 annular volumes, typical simulations took approximately 10 minutes on a single CPU.

FIGURES

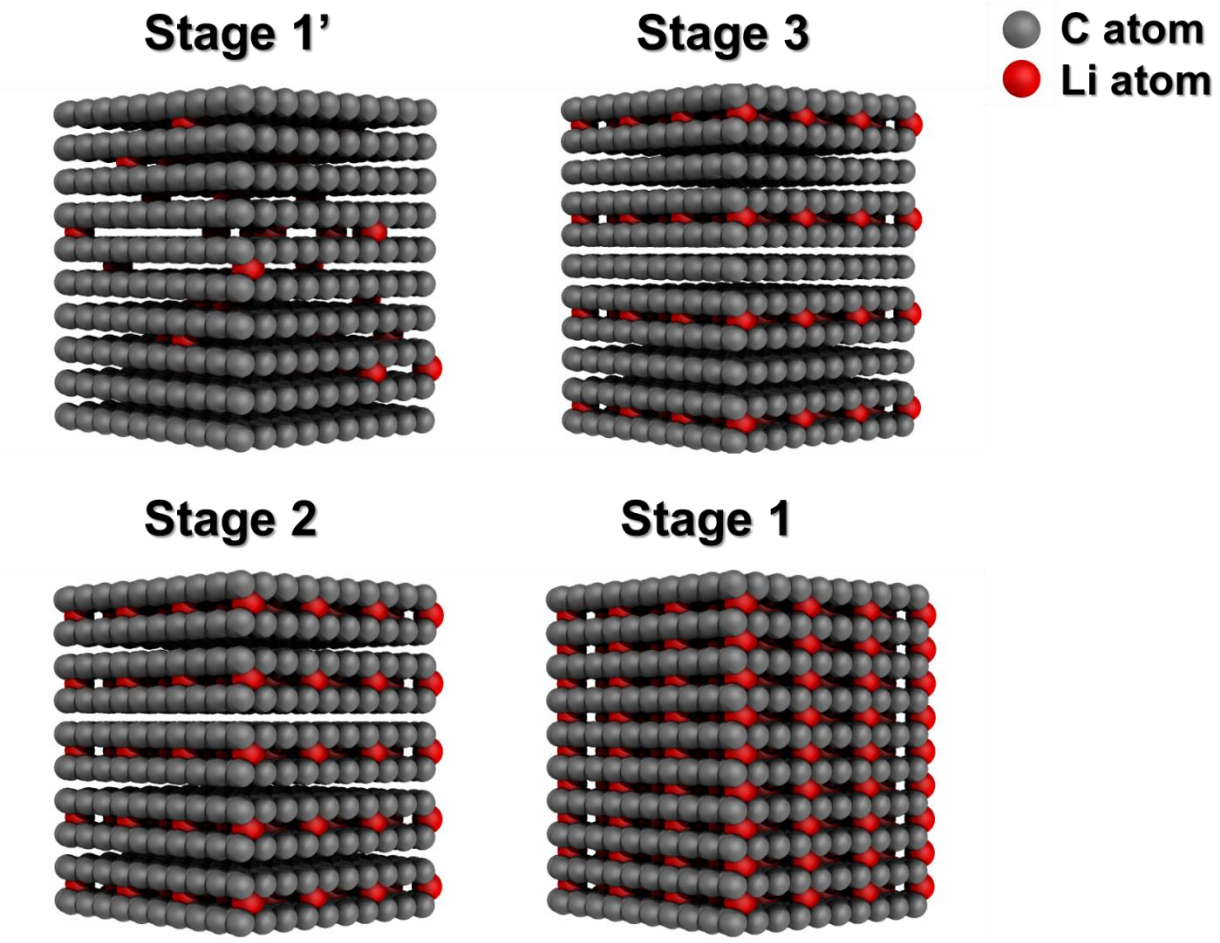

Figure 1. Thermodynamic stages during Li intercalation (from Li_xC_6 phase diagram[18]). Stage 1' denotes a dilute stage 1 at very low Li concentrations.

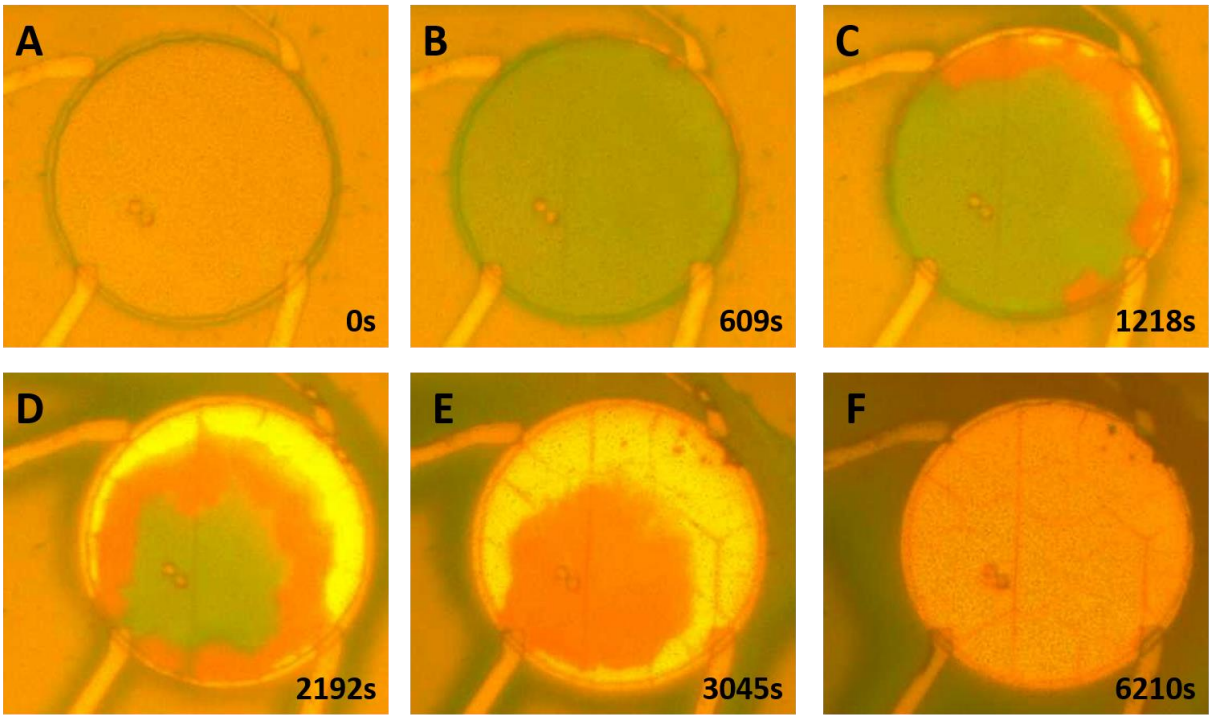

Figure 2. Sequential color images of Li intercalation into a 50 μm diameter graphite disk: dilute stage 1'(A), stage 3(B), stages 3, 2, and 1(C), stages 3, 2, and 1(D), stages 2 and 1(E), and finally complete stage 1(F). Time is indicated in seconds. Colorations around the graphite edge and the Ti metallic leads are attributed to side redox reactions with polymer electrolyte. Throughout the intercalation, an external -5V voltage step was applied (also discussed in Supporting Information).

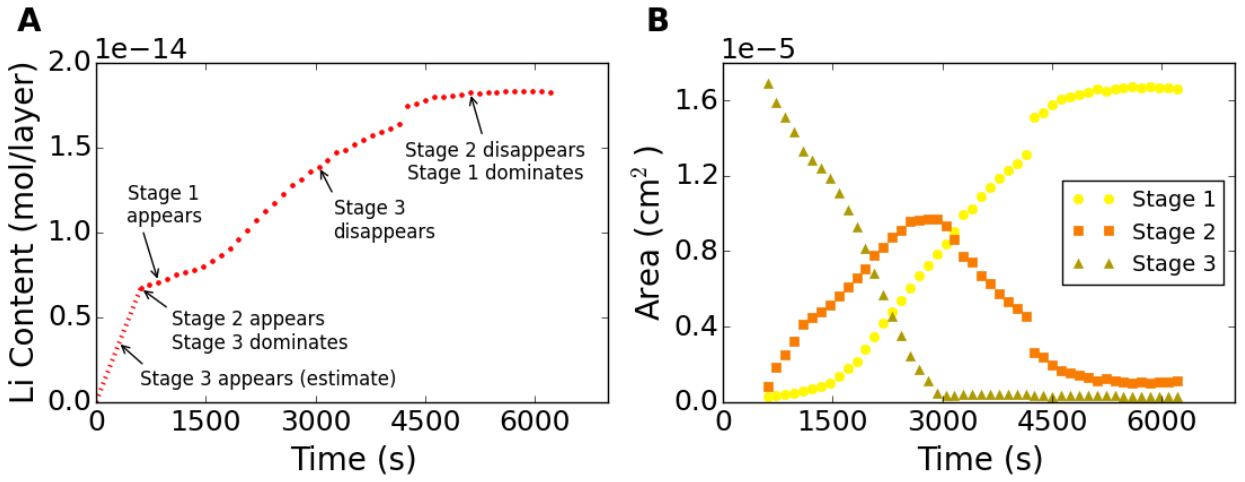

Figure 3. Direct optical measurement of Li intercalation kinetics. Both the total content of Li within the graphite disc (Figure 3A) and the area of the distinct stages (Figure 3B) are obtained from optical images by image segmentation.

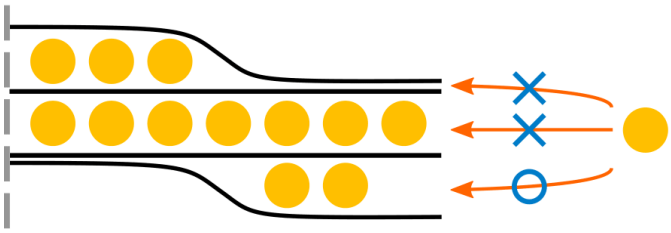

Figure 4: Proposed injection mechanism of Li from the electrolyte into the graphite disk at the edge: graphene planes are black and Li ions are yellow circles. The presence of Li expands the layer to layer separation. Only the bottom injection process (marked with a circle) occurs. Li insertion is blocked in the top path because the graphene layers have collapsed. In the middle, there is no available site. In the bottom, there is an available site and a nearby intercalant in the same layer, promoting reaction.

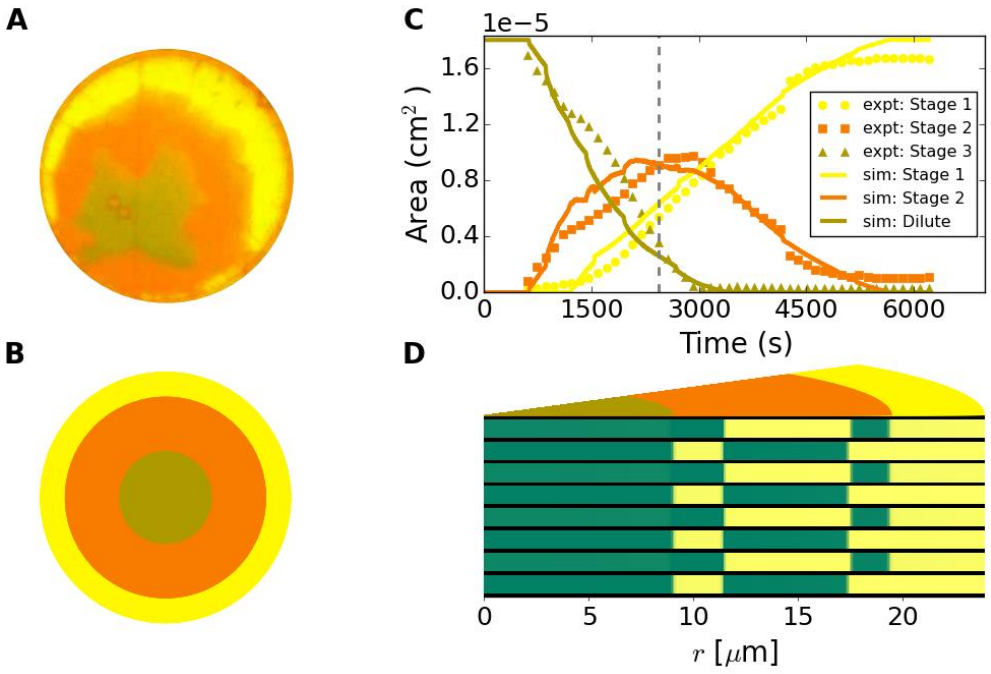

Figure 5: Comparison of experiment (A, C) and a simulation snapshot (B, C, D). The inner green region is stage 3 (Dilute 1' in the simulation), the middle red ring is stage 2, and the outer yellow ring is stage 1. In C, the stage areas are plotted versus time for the experiment (Figure 3, points) and simulation (lines). The diagram in D shows the concentration profiles from the simulation. The 2 different simulated layers are repeated for visual clarity in a cross-sectional slice. Black lines represent graphene planes, and green/yellow regions between represent empty/full lithium sites. The top view (B, D) is colored according to the calculated concentration profiles. The simulation shows phase separation within each intralayer space, as well as (in the red region) a preference for a Daumas-Hérold domains[30] with a "checkerboard" filling pattern.

ASSOCIATED CONTENT

Supporting Information. Device schematic and reaction initiation, overpotential analysis, electrochemical device characterization, time lapse movie, Raman characterization, and theory. This material is available free of charge via the Internet at http://pubs.acs.org.

AUTHOR INFORMATION

Corresponding Author

Louis Brus

leb26@columbia.edu

Present Addresses

†If an author's address is different than the one given in the affiliation line, this information may be included here.

ACKNOWLEDGMENT

We would like to thank Michael Steigerwald, Haitao Liu, Andrew Crowther, Zheyuan Chen, Naeyoung Jung, Elizabeth Thrall and Archana Raja for helpful discussions. We would like to thank Dezheng Sun for experimental assistance. This project was supported by primarily through the Center for Re-Defining Photovoltaic Efficiency Through Molecular-Scale Control, an Energy Frontier Research Center (EFRC) funded by the U.S. Department of Energy, Office of Science, Office of Basic Energy Sciences under award DE-SC0001085. P.K. acknowledges support from DMREF grant from National Science Foundation (NSF) DMR-1435487. R. B. S. and M. Z. B. acknowledge support from the Samsung Advanced Institute of Technology.

REFERENCES

(1) Dresselhaus, M. S.; Dresselhaus, G. Intercalation Compounds of Graphite. *Advances in Physics* **2002**, *51*, 1–186.

(2) Aurbach, D. Common Electroanalytical Behavior of Li Intercalation Processes into Graphite and Transition Metal Oxides. *Journal of the Electrochemical Society* **1998**, *145*, 3024.

(3) Persson, K.; Hinuma, Y.; Meng, Y. S.; Van der Ven, A.; Ceder, G. Thermodynamic and Kinetic Properties of the Li-Graphite System from First-Principles Calculations. *Physical Review B* **2010**, *82*, 125416.

(4) Persson, K.; Sethuraman, V. a.; Hardwick, L. J.; Hinuma, Y.; Shirley, Y.; Ven, A. Van Der; Srinivasan, V.; Kostecki, R.; Ceder, G.; Berkeley, L.; et al. Lithium Diffusion in Graphitic Carbon. *The Journal of Physical Chemistry Letters* **2010**, *1*, 1176–1180.

(5) Yao, F.; Güneş, F.; Ta, H. Q.; Lee, S. M.; Chae, S. J.; Sheem, K. Y.; Cojocaru, C. S.; Xie, S. S.; Lee, Y. H. Diffusion Mechanism of Lithium Ion through Basal Plane of Layered Graphene. *Journal of the American Chemical Society* **2012**, *134*, 8646–8654.

(6) Levi, M. D.; Aurbach, D. The Application of Electroanalytical Methods to the Analysis of Phase Transitions during Intercalation of Ions into Electrodes. *Journal of Solid State Electrochemistry* **2007**, *11*, 1031–1042.

(7) Van der Ven, A.; Bhattacharya, J.; Belak, A. a. Understanding Li Diffusion in Li-Intercalation Compounds. *Accounts of Chemical Research* **2012**, *46*, 1216–1225.

(8) Reynier, Y. F.; Yazami, R.; Fultz, B. Thermodynamics of Lithium Intercalation into Graphites and Disordered Carbons. *Journal of The Electrochemical Society* **2004**, *151*, A422–A426.

(9) Grey, C. P.; Dupré, N. NMR Studies of Cathode Materials for Lithium-Ion Rechargeable Batteries. *Chemical Reviews* **2004**, *104*, 4493–4512.

(10) Migge, S.; Sandmann, G.; Rahner, D.; Dietz, H.; Plieth, W. Studying Lithium Intercalation into Graphite Particles via in Situ Raman Spectroscopy and Confocal Microscopy. *Journal of Solid State Electrochemistry* **2004**, *9*, 132–137.

(11) Ferguson, T. R.; Bazant, M. Z. Nonequilibrium Thermodynamics of Porous Electrodes. *Journal of the Electrochemical Society* **2012**, *159*, A1967–A1985.

(12) Ferguson, T. R.; Bazant, M. Z. Phase Transformation Dynamics in Porous Battery Electrodes. *Electrochimica Acta* **2014**, *146*, 89–97.

(13) Li, Y.; El Gabaly, F.; Ferguson, T. R.; Smith, R. B.; Bartelt, N. C.; Sugar, J. D.; Fenton, K. R.; Cogswell, D. A.; Kilcoyne, A. L. D.; Tyliszczak, T.; et al. Current-Induced Transition from Particle-by-Particle to Concurrent Intercalation in Phase-Separating Battery Electrodes. *Nature Materials* **2014**, *13*, 1149–1156.

(14) Yu, P.; Popov, B. N.; Ritter, J. A.; White, R. E. Determination of the Lithium Ion Diffusion Coefficient in Graphite. *Journal of The Electrochemical Society* **1999**, *146*, 8.

(15) Harris, S. J.; Timmons, A.; Baker, D. R.; Monroe, C. Direct in Situ Measurements of Li Transport in Li-Ion Battery Negative Electrodes. *Chemical Physics Letters* **2010**, *485*, 265–274.

(16) Maire, P.; Kaiser, H.; Scheifele, W.; Novák, P. Colorimetric Determination of Lithium-Ion Mobility in Graphite Composite Electrodes. *Journal of Electroanalytical Chemistry* **2010**, *644*, 127–131.

(17) Ohzuku, T. Formation of Lithium-Graphite Intercalation Compounds in Nonaqueous Electrolytes and Their Application as a Negative Electrode for a Lithium Ion (Shuttlecock) Cell. *Journal of The Electrochemical Society* **1993**, *140*, 2490.

(18) Dahn, J. R. Phase Diagram of LixC6. *Physical Review B* **1991**, *44*, 9170–9177.

(19) Fischer, J. E.; Bloch, J. M.; Shieh, C. C.; Preil, M. E.; Jelley, K. Reflectivity Spectra and Dielectric Function of Stage-1 Donor Intercalation Compounds of Graphite. *Physical Review B* **1985**, *31*, 4773–4783.

(20) Yang, M.; Eklund, P. Optical Dielectric Function of High-Stage Potassium Graphite Intercalation Compounds: Experiment and Theory. *Physical Review B* **1988**, *38*, 3505–3516.

(21) Zanini, M.; Basu, S.; Fischer, J. E. Alternate Synthesis and Reflectivity Spectrum of Stage 1 Lithium-Graphite Intercalation Compound. *Carbon* **1978**, *16*, 211–212.

(22) Zanini, M.; Fischer, J. Polarized Reflectance of Alkali Metal-Graphite Intercalation Compounds. *Materials Science and Engineering* **1977**, *31*, 169–172.

(23) Shi, Q.; Dokko, K.; Scherson, D. A. In Situ Raman Microscopy of a Single Graphite Microflake Electrode in a Li+-Containing Electrolyte. *The Journal of Physical Chemistry B* **2004**, *108*, 4789–4793.

(24) Levi, M. D.; Markevich, E.; Wang, C.; Aurbach, D. Chronoamperometric Measurements and Modeling of Nucleation and Growth, and Moving Boundary Stages during Electrochemical Lithiation of Graphite Electrode. *Journal of Electroanalytical Chemistry* **2007**, *600*, 13–22.

(25) Coulet, A.; Bouche, K.; Marinelli, F.; Barbier, F. Growth Kinetics of Intermediate Compounds at a Planar Solid-Solid or Solid-Liquid Interface by Diffusion Mechanisms. *Journal of Applied Physics* **1997**, *82*, 6001.

(26) Funabiki, A.; Inaba, M.; Abe, T.; Ogumi, Z. Stage Transformation of Lithium-Graphite Intercalation Compounds Caused by Electrochemical Lithium Intercalation. *Journal of the Electrochemical Society* **1999**, *146*, 2443–2448.

(27) Wagner, C. The Evaluation of Data Obtained with Diffusion Couples of Binary Single-Phase and Multiphase Systems. *Acta Metallurgica* **1969**, *17*, 99–107.

(28) Bazant, M. Z. Theory of Chemical Kinetics and Charge Transfer Based on Nonequilibrium Thermodynamics. *Accounts of Chemical Research* **2013**, *46*, 1144–1160.

(29) Zeng, Y.; Bazant, M. Z. Phase Separation Dynamics in Isotropic Ion-Intercalation Particles. *SIAM Journal on Applied Mathematics* **2014**, *74*, 980–1004.

(30) Daumas, N.; Herold, A. Sur Les Relations Entre La Notion de Stade et Les Mecanismes Reactionnels Dans Les Composes D'insertion Du Graphite. *Comptes Rendus de l'Académie des Sciences de Paris* **1969**, *268*, 373–375.

(31) Safran, S. A. Phase Diagrams for Staged Intercalation Compounds. *Physical Review Letters* **1980**, *44*, 937.

(32) Kirczenow, G. Kinetics of Stage Ordering and Stage Transitions. *Physical Review Letters* **1985**, *55*, 2810.

(33) Krishnan, S.; Brenet, G.; Machado-Charry, E.; Caliste, D.; Genovese, L.; Deutsch, T.; Pochet, P. Revisiting the Domain Model for Lithium Intercalated Graphite. *Applied Physics Letters* **2013**, *103*, 251904.

(34) Thomas, J. M.; Millward, G. R.; Schlogl, R. F.; Boehm, H. P. Direct Imaging of a Graphite Intercalate: Evidence of Interpenetation of "Stages" in Graphite: Ferric Chloride. *Materials Research Bulletin* **1980**, *15*, 671–676.

(35) Dimiev, A. M.; Ceriotti, G.; Behabtu, N.; Zakhidov, D.; Pasquali, M.; Saito, R.; Tour, J. M. Direct Real-Time Monitoring of Stage Transitions in Graphite Intercalation Compounds. *ACS Nano* **2013**, *7*, 2773–2780.

(36) Heß, M.; Novák, P. Shrinking Annuli Mechanism and Stage-Dependent Rate Capability of Thin-Layer Graphite Electrodes for Lithium-Ion Batteries. *Electrochimica Acta* **2013**, *106*, 149–158.

(37) Safran, S. A.; Hamann, D. R. Long-Range Elastic Interactions and Staging in Graphite Intercalation Compounds. *Physical Review Letters* **1979**, *42*, 1410–1413.

(38) Kganyago, K. R.; Ngoepe, P. E. Structural and Electronic Properties of Lithium Intercalated Graphite LiC6. *Physical Review B* **2003**, *68*, 205111.

(39) Di Leo, C. V; Rejovitzky, E.; Anand, L. A Cahn–Hilliard-Type Phase-Field Theory for Species Diffusion Coupled with Large Elastic Deformations: Application to Phase-Separating Li-Ion Electrode Materials. *Journal of the Mechanics and Physics of Solids* **2014**, *70*, 1–29.

(40) Hawrylak, P.; Subbaswamy, K. R. Kinetic Model of Stage Transformation and Intercalation in Graphite. *Physical Review Letters* **1984**, *53*, 2098.

(41) Blake, P.; Hill, E.; Neto, A.; Novoselov, K. Making Graphene Visible. *Applied Physics Letters* **2007**, 13–15.

(42) Sorgenfrei, S.; Chiu, C.; Gonzalez, R. L.; Yu, Y.-J.; Kim, P.; Nuckolls, C.; Shepard, K. L. Label-Free Single-Molecule Detection of DNA-Hybridization Kinetics with a Carbon Nanotube Field-Effect Transistor. *Nature Nanotechnology* **2011**, *6*, 126–132.

(43) Ichino, T.; Cahan, B. D.; Scherson, D. A. In Situ Attenuated Total Reflection Fourier Transform Infrared Spectroscopy Studies of the Polyethylene Oxide/LiClO4-Metallic

Lithium Interface. *Jounral of the Electrochemical Society* **1991**, *138*, 59–61.

(44) Implemented in Scipy 0.12.0 Library as the scipy.cluster.vq.kmeans2 Function, and in MATLAB R2012a as the Kmeans Function.

(45) Nikolić, D. D. DAE Tools: Equation-Based Object-Oriented Modelling, Simulation and Optimisation Software. *PeerJ Computer Science* **2016**, *2*, e54.

(46) Hindmarsh, A. C. SUNDIALS Suite of Nonlinear and Differential/algebraic Equation Solvers. *ACM transactions on mathematical software* **2005**, *31*, 363–396.

(47) Griewank, A.; Juedes, D.; Utke, J. Algorithm 755: ADOL-C: A Package for the Automatic Differentiation of Algorithms Written in C/C++. *ACM Trans. Math. Softw.* **1996**, *22*, 131–167.

Li Intercalation into Graphite: Direct Optical Imaging and Cahn-Hilliard Reaction Dynamics

Yinsheng Guo[1], Raymond B. Smith[2], Zhonghua Yu[1], Dmitri K. Efetov[3], Junpu Wang[3], Philip Kim[3], Martin Z. Bazant[2, 4], Louis E. Brus[1]

[1]Department of Chemistry and [3]Department of Physics, Columbia University, New York, 10027, United States

[2]Department of Chemical Engineering and [4]Department of Mathematics, Massachusetts Institute of Technology, Cambridge, Massachusetts, 02139, United States

Supporting information

Device schematic and reaction initiation

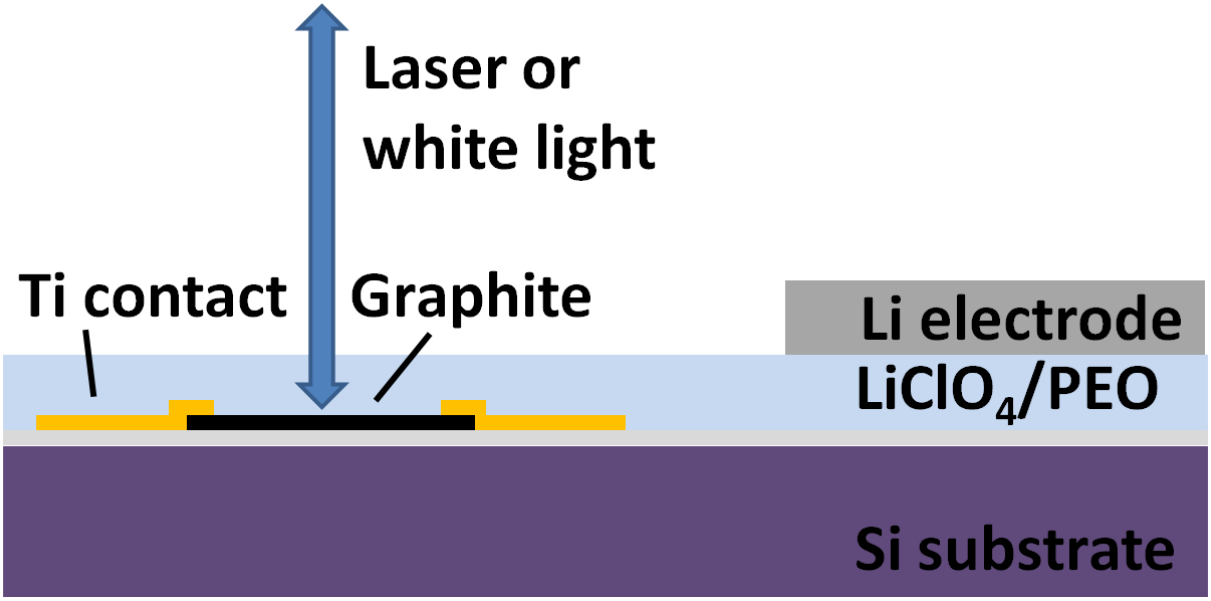

Figure S1 shows the schematic diagram of our experimental device. The open circuit voltage of our micro device was 0V. This was the equilibrium voltage established with Titanium contact and graphite disc against Li metal. Full lithium intercalation was achieved with a -5V step voltage applied to the device.

Li intercalation reaction was initiated by applying a -5V step voltage to the device. We studied the voltage dependence of reaction initiation by applying a series of step voltages. Intercalation proceeded ultimately to stage 1 for applied voltages higher than -4V. Below this threshold voltage, we only saw partial intercalation with low concentration phases.

Apparent high overpotential and parallel reaction model

The high observed overpotential appears to be a consequence of the nonlinear Butler-Volmer relationship between voltage and resistance, combined with a side reaction preceding the energetic intercalation reaction. This overpotential is not fully characterized.

The equivalent circuit of our device consists of an internal resistance (e.g. electrolyte and contact resistances) in series with the parallel combination of two electrochemical reactions: Li intercalation and the working electrode/electrolyte surface reaction.

The resistance of the two parallel reactions is described by separate Butler-Volmer equations. At high potential, both reactions are highly resistive with negligible currents. As the potential drops,

the side reaction reducing the electrolyte on the electrode surface precedes the Li intercalation reaction. In other words, the side reaction has a higher potential vs. Li/Li+ than the intercalation. The side reaction resistance drops exponentially as its threshold is exceeded. This effectively shorts the intercalation reaction, and makes the high internal resistance a more dominating element in the equivalent circuit. Beyond this point, extra voltage applied is mainly dissipated by the electrolyte and side reactions, rather than the intercalation element, and thus little interfacial current goes toward intercalation. The combination of these aspects results in the apparent high overpotential needed to turn on the Li intercalation in our experiments.

This type of behavior has been extensively observed as the Solid-Electrolyte Interphase formation preceding the first charging cycle in Li-ion batteries.

This circuit model can quantitatively reproduce the observed high overpotential. We note that the Butler-Volmer equation loses accuracy in the large overpotential regime and tends to overestimate the current (underestimate the resistance) compared to Marcus theory of charge transfer, as revealed by recent experiments on Li intercalation.[1] However the qualitative explanation of the large voltage would be unchanged. A more complete development of these ideas is presently underway.

Electrochemical device characterization

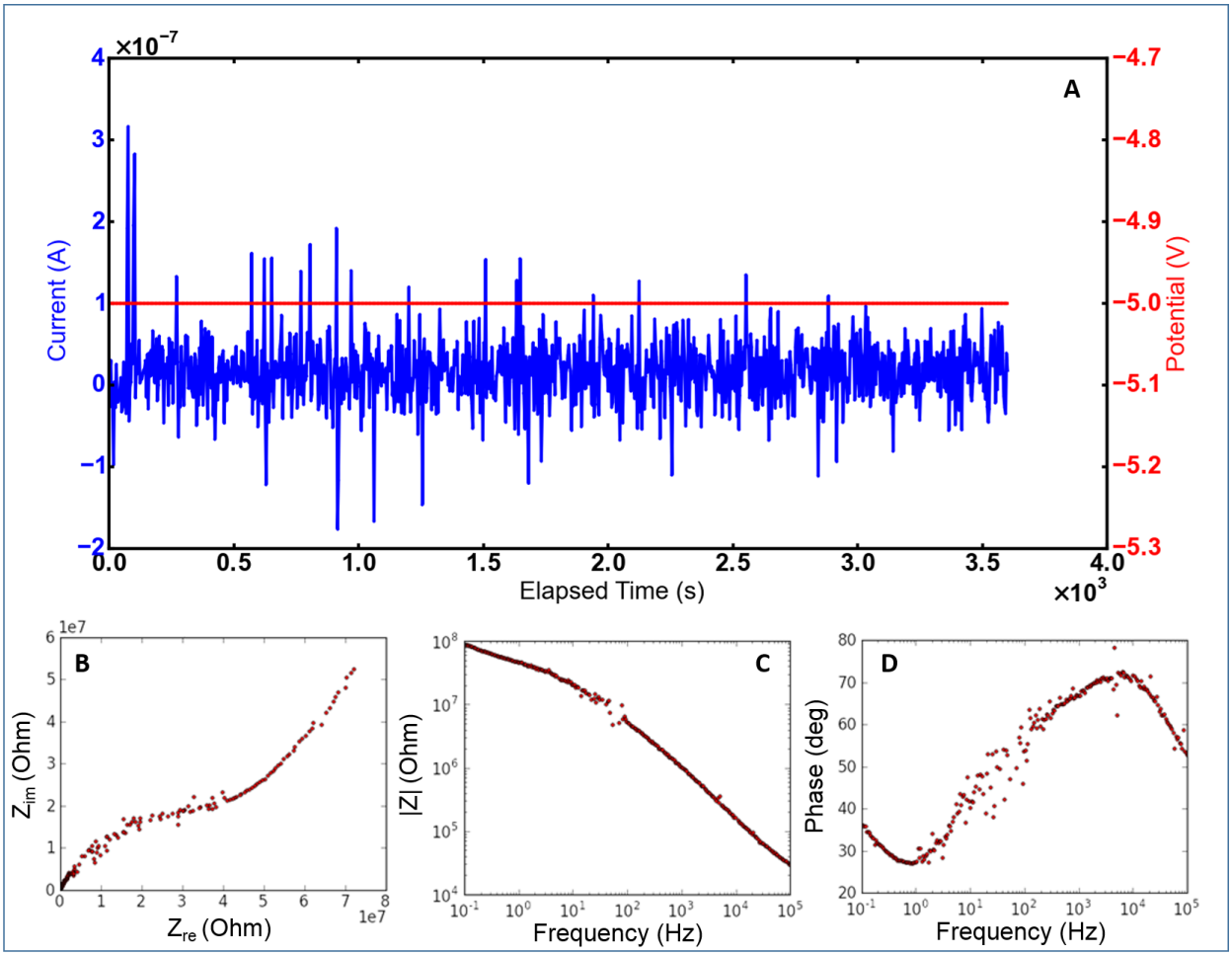

Figure S2. Electrochemical characterization of the microscopic single-flake device. A) Chronoamperometry trace during Li intercalation. A -5V voltage step (red) was applied B), C), and D) Electrochemical impedance spectroscopy of a typical device before Li intercalation, at the 0V open circuit voltage.

Figure S2 shows electrochemical characterization of the microscopic single-flake devices used in the intercalation measurements. Figure S2A plots the voltage-time and current-time traces during Li intercalation, after a step voltage was applied. The measured I-t trace shows no clear structured features related to the graphite intercalation stage transformation. Because we study a micron-sized single flake, rather than a macroscopic graphite electrode, side reactions and film formation should generate currents orders of magnitude larger than the intrinsic intercalation current. Despite the absence of intercalation current features, we can directly probe the intercalation kinetics by all-optical measurements as described in the text. Figure S2B, C, and D give an overview of the electrochemical characteristics of the device before Li intercalation. The microscopic device showed very high impedance under the open circuit condition, compared with macroscopic cells.[2,3]

Time lapse movie

A movie of Li intercalation is compiled from time lapse imaging data, and is available in the attachment.

Raman Characterization

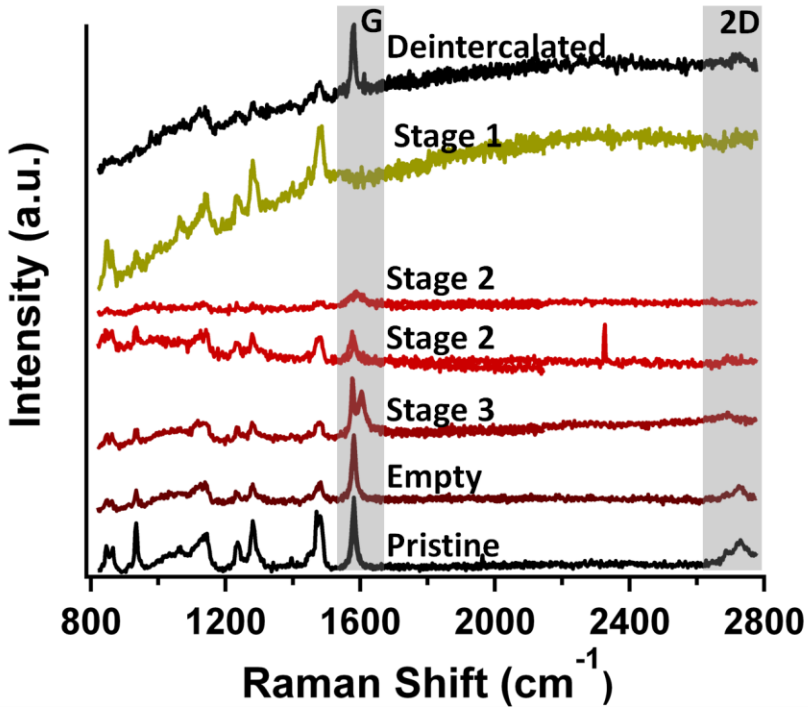

Figure S3. Raman spectra of Li – graphite intercalation system in different stages. The spectra are vertically offset for a clearer display. The peak near 1580cm^{-1} is the graphite G peak. The peak around 2700cm^{-1} is the graphite 2D peak. The peaks below G peak are from PEO and P(EO)-Li complexes.[4] Stage 1 intercalation compound was achieved with external applied voltage at -5V.

Phase assignments are confirmed by Raman spectra in figure S3. The graphene G peak near 1580 cm^{-1} shows electronic resonance intensity enhancement and shifts to higher frequency with the concentration of free in-plane graphite electrons. It is diagnostic for electronic structure, clearly evolving from one phase to the next. For n=3 and higher stages, the G peak splits into two as there are two physically inequivalent graphene layers: highly doped graphene in direct contact with intercalated Li , and interior graphene with little doping, similar to pristine graphite. Similar two-peak Raman spectra have been recently observed in few layer graphenes with

adsorbed NO_2, which is a strong electron acceptor.[5] For stage 2 GIC, in which all graphene layers are equivalent, there is only one G peak with weaker intensity. It is softened to a lower frequency than the direct contact G peak in stage 3, indicating a higher doping level in stage 2, explained by an in plane lattice expansion accompanying such higher doping[6]. For stage 1, the G mode is absent. This vanishing behavior, and the weak intensity of the G mode in stage 2, in part occur because of a loss of electronic resonance Raman enhancement, which occurs as the interband visible optical absorption bleaches for Fermi level shifts of about 1 eV. Note that several theoretical calculations indicate that stage 1 LiC_6 charge transfer from Li atom to graphene approaches 100%.[7,8]

Theory

The free energy density of each layer is modeled as a regular solution with a gradient energy penalty,

$$g_\ell(c) = c_{max}\{k_B T[c\ln(c) + (1-c)\ln(1-c)] + \Omega_a c(1-c) + c\mu^\ominus\} + \frac{1}{2}\kappa(\nabla c)^2, \quad \text{(S1)}$$

and the total free energy density is given by the sum of the two layers' free energy densities and interaction energies,

$$g = g_\ell(c_1) + g_\ell(c_2) + c_{max}[\,\Omega_b c_1 c_2 + \Omega_c c_1(1-c_1)c_2(1-c_2)], \quad \text{(S2)}$$

where c_{max} is the maximum concentration of lithium within a layer, k_B is the Boltzmann constant, T is the absolute temperature, c_i is the local filling fraction in layer i, Ω_a is the regular solution interaction of particles and holes within a layer, κ is the gradient energy penalty, Ω_b penalizes regions in which adjacent layers are full, and Ω_c penalizes regions in which adjacent layers are both in intermediate filling fractions. Chemical potentials μ_i in each layer are obtained from a variational derivative of the free energy with respect to the layer concentration. The thermodynamic treatment is similar to that in previous work describing staging dynamics in graphite[9–11]. For a review of work on graphite staging dynamics, see reference below[12].

For our reaction boundary condition in each layer, we implement a thermodynamically consistent version of the symmetric Butler-Volmer equation[13]. Assuming unit activity of lithium in the electrolyte and defining V_{set} to be the difference between the standard (defined by Eq. S1 and S2) and applied interfacial voltage,

$$-\hat{n}\cdot(F_i)_s = \frac{k_0}{2\gamma_{\ddagger,i}}\left[\exp\left(\frac{eV_{set}}{2k_BT}\right) - a_R\exp\left(-\frac{eV_{set}}{2k_BT}\right)\right] \approx \frac{k_{eff}}{2\gamma_{\ddagger,i}} \quad \text{(S3)}$$

where $\hat{n}$ is a unit outward pointing normal vector, $(F_i)_s$ is the flux at the particle surface in layer i, k_0 is the reaction rate constant per unit reacting surface area, $\gamma_{\ddagger,i}$ is the activity coefficient of the reaction transition state, e is the elementary charge, and a_R is the activity of intercalated lithium at the surface (from Eq. S1 and S2). The last expression comes from assuming the rate of reduction is much faster than that of oxidation, which is true for the large majority of the simulation and results in an effective reaction parameter, $k_{eff} = k_0\exp(eV_{set}/2k_BT)$. We find simulation results are primarily sensitive to this lumped parameter rather than k_0 and V_{set} independently. The

description is completed by our model for the activity coefficient for the transition state, which is discussed in the main text. Mathematically,

$$\gamma_{\ddagger,i} = \frac{1}{c_{i,s}(1-c_{i,s})} \tag{S4}$$

where $c_{i,s}$ is the filling fraction of lithium at the surface of layer i. This expression is a result of assuming the activity of the transition state is described simply by entropic effects, and a transition state can only be placed at a surface site in which there is both a particle and a hole nearby.[13] Other reasonable assumptions for the transition state could be (1) simple dilute solution, $\gamma_{\ddagger,i} = 1$, (2) requiring only a nearby hole, $\gamma_{\ddagger,i} = 1/(1 - c_{i,s})$, (3) requiring a hole in both layers, $\gamma_{\ddagger,i} = 1/(1 - c_{1,s})(1 - c_{2,s})$, (4) requiring both a hole and particle in both layers, $\gamma_{\ddagger,i} = 1/(c_{1,s}(1 - c_{1,s})c_{2,s}(1 - c_{2,s}))$, (5) or requiring only a nearby particle, $\gamma_{\ddagger,i} = 1/c_{i,s}$. None of these alternatives provided fits as close to the data as the model requiring a nearby hole and particle in the reacting layer, as in Eq. S4.

We note that the above formulation assumes constant concentration and electric potential in the electrolyte around the graphite disc. A more complete formulation could account for electrolyte transport, which we neglect here for simplicity. A rough estimation of the limiting current in the electrolyte compared to experimentally measured electrical current through the outer circuit suggests that electroltye transport could have a non-trivial effect and could be related, e.g., to the breaking of symmetry in the injection around the disc. However, symmetry could also be broken in other ways such as by random buckling of the particle in the c-direction near the surface, residuals on the circumference from lithographic processes, and other heterogeneities in the reaction rate constant around the disc surface, all of which would be challenging to model accurately. As such, we opted instead to keep the model as simple as possible while obtaining a reasonable description of the experimental results.

The chemical diffusivity in each layer is derived here for near-equilibrium cases in which the system has only small conentration gradients. Equation S5 (previously derived[13]) gives $D_{chem,i}$, which is an effective chemical diffusivity within one layer assuming small concentration gradients. This is expanded in equation S6 using the homogeneous Li/graphite free energy density (Figure S4),

$$D_{chem,i} = \frac{D_0}{k_B T} c_{max}(1 - c_i)c_i \frac{\partial \mu_i}{\partial c_i} \tag{S5}$$

$$= \frac{D_0}{k_B T}\left[k_B T - 2\Omega_a c_i(1 - c_i) - 2\Omega_c c_i(1 - c_i)c_j(1 - c_j)\right], \tag{S6}$$

such that the flux within each layer, $F_i = -D_{chem,i}\nabla c_i$.

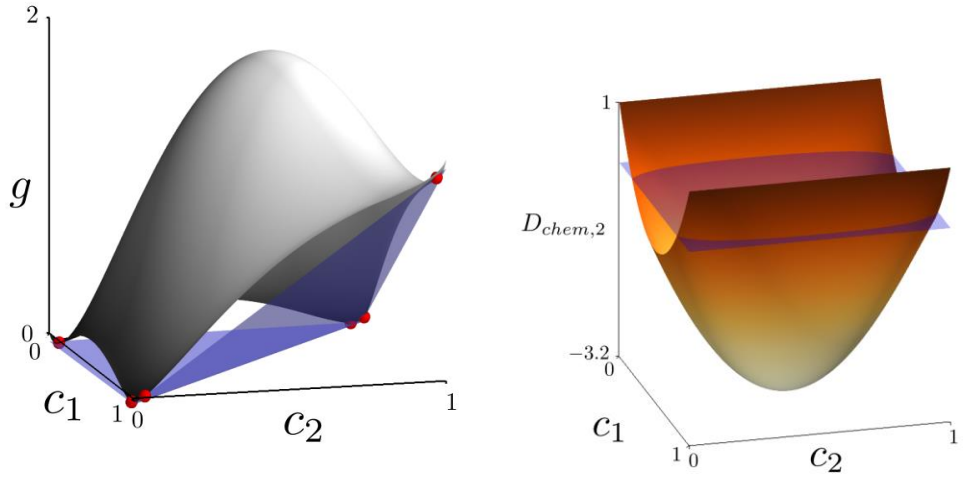

Figure S4: Concentration dependence of (a) local homogeneous free energy density, and (b) chemical diffusivity within a single layer. The common tangent planes in (a) meet the surface at the red points, which represent the equilibrium concentrations for overall concentrations lying within the miscibility gap. In (b), the chemical diffusivity is scaled to the dilute limit tracer diffusivity, D_0.

Finally, the simulation was carried out by imposing a time ramp on the voltage, $V = V_{set} \tanh\frac{t}{450\ s}$, which was done for numerical convenience to emulate a nearly-pristine initial graphite. Simulation results with initial solid filling fractions of 10^{-15} and no time ramp $V = V_{set}$ were very similar to those using a time ramp with initial filling fractions of 0.01. However, those with such low concentration initial conditions required extremely tight tolerances and took considerably longer to run. A table of all parameter values used in the simulation is presented in Table S1.

Parameter	Value	Note
D_0	1.25×10^{-12} cm^2/s	Dilute limit tracer diffusivity, adjusted slightly from ref. [14]
k_0	0.03 A/m^2	Fit (Adjusted with Vset)
V_{set}	0.5 V	See discussion in text
Ω_a	8.43 kJ/mol	From ref. [15]
Ω_b	3.47 kJ/mol	From ref. [15]

Ω_c	49.6 kJ/mol	From ref. [15]
κ	4×10^{-7} J/m	Results not sensitive to value
T	298 K	Room temperature

References

(1) Bai, P.; Bazant, M. Z. Charge Transfer Kinetics at the Solid-Solid Interface in Porous Electrodes. *Nature Communications* **2014**, *5*, 3585.

(2) Funabiki, A.; Inaba, M.; Ogumi, Z.; Yuasa, S.; Otsuji, J.; Tasaka, A. Impedance Study on the Electrochemical Lithium Intercalation into Natural Graphite Powder. *Journal of The Electrochemical Society* **1998**, *145*, 172–178.

(3) Wang, C.; Appleby, A. J.; Little, F. E. Electrochemical Impedance Study of Initial Lithium Ion Intercalation into Graphite Powders. *Electrochimica Acta* **2001**, *46*, 1793–1813.

(4) Ducasse, L.; Dussauze, M.; Grondin, J.; Lassègues, J.-C.; Naudin, C.; Servant, L. Spectroscopic Study of Poly(ethylene oxide)6: LiX Complexes (X = PF6, AsF6, SbF6, ClO4). *Physical Chemistry Chemical Physics* **2003**, *5*, 567–574.

(5) Crowther, A. C.; Ghassaei, A.; Jung, N.; Brus, L. E. Strong Charge-Transfer Doping of 1 to 10 Layer Graphene by NO2. *ACS Nano* **2012**, *6*, 1865–1875.

(6) Dresselhaus, M. S.; Dresselhaus, G. Intercalation Compounds of Graphite. *Advances in Physics* **2002**, *51*, 1–186.

(7) Csányi, G.; Littlewood, P. B.; Nevidomskyy, A. H.; Pickard, C. J.; Simons, B. D. The Role of the Interlayer State in the Electronic Structure of Superconducting Graphite Intercalated Compounds. *Nature Physics* **2005**, *1*, 42–45.

(8) Profeta, G.; Calandra, M.; Mauri, F. Phonon-Mediated Superconductivity in Graphene by Lithium Deposition. *Nature Physics* **2012**, *8*, 131–134.

(9) Hawrylak, P.; Subbaswamy, K. R. Kinetic Model of Stage Transformation and Intercalation in Graphite. *Physical Review Letters* **1984**, *53*, 2098.

(10) Safran, S. A. Phase Diagrams for Staged Intercalation Compounds. *Physical Review Letters* **1980**, *44*, 937.

(11) Kirczenow, G. Kinetics of Stage Ordering and Stage Transitions. *Physical Review Letters* **1985**, *55*, 2810.

(12) Kirczenow, G. Staging and Kinetics. In *Graphite Intercalation Compounds I SE - 3*; Zabel, H., Solin, S., Eds.; Springer Series in Materials Science; Springer Berlin Heidelberg, 1990; Vol. 14, pp 59–100.

(13) Bazant, M. Z. Theory of Chemical Kinetics and Charge Transfer Based on Nonequilibrium Thermodynamics. *Accounts of Chemical Research* **2013**, *46*, 1144–1160.

(14) Persson, K.; Hinuma, Y.; Meng, Y. S.; Van der Ven, A.; Ceder, G. Thermodynamic and Kinetic Properties of the Li-Graphite System from First-Principles Calculations. *Physical Review B* **2010**, *82*, 125416.

(15) Ferguson, T. R.; Bazant, M. Z. Phase Transformation Dynamics in Porous Battery Electrodes. *Electrochimica Acta* **2014**, *146*, 89–97.